

# SCIENTIFIC REPORTS

OPEN

## Volcanic influence on centennial to millennial Holocene Greenland temperature change

Takuro Kobashi<sup>1,2,10</sup>, Laurie Menviel<sup>3,4</sup>, Aurich Jeltsch-Thömmes<sup>1,2</sup>, Bo M. Vinther<sup>5</sup>, Jason E. Box<sup>6</sup>, Raimund Muscheler<sup>7</sup>, Toshiyuki Nakaegawa<sup>8</sup>, Patrik L. Pfister<sup>1,2</sup>, Michael Döring<sup>1,2</sup>, Markus Leuenberger<sup>1,2</sup>, Heinz Wanner<sup>2</sup> & Atsumu Ohmura<sup>9</sup>

Solar variability has been hypothesized to be a major driver of North Atlantic millennial-scale climate variations through the Holocene along with orbitally induced insolation change. However, another important climate driver, volcanic forcing has generally been underestimated prior to the past 2,500 years partly owing to the lack of proper proxy temperature records. Here, we reconstruct seasonally unbiased and physically constrained Greenland Summit temperatures over the Holocene using argon and nitrogen isotopes within trapped air in a Greenland ice core (GISP2). We show that a series of volcanic eruptions through the Holocene played an important role in driving centennial to millennial-scale temperature changes in Greenland. The reconstructed Greenland temperature exhibits significant millennial correlations with  $K^+$  and  $Na^+$  ions in the GISP2 ice core (proxies for atmospheric circulation patterns), and  $\delta^{18}O$  of Oman and Chinese Dongge cave stalagmites (proxies for monsoon activity), indicating that the reconstructed temperature contains hemispheric signals. Climate model simulations forced with the volcanic forcing further suggest that a series of large volcanic eruptions induced hemispheric-wide centennial to millennial-scale variability through ocean/sea-ice feedbacks. Therefore, we conclude that volcanic activity played a critical role in driving centennial to millennial-scale Holocene temperature variability in Greenland and likely beyond.

Holocene climate variability is important to understand the process of human societal development from a hunter-gatherer society to the present complex society<sup>1,2</sup>. However, precise understanding of Holocene climate variability on multidecadal to millennial scales has been elusive owing to the lack of adequate archives recording small temperature signals and poorer chronologies further back in time<sup>3</sup>. Therefore, we employed a relatively newly established method of temperature reconstruction using argon and nitrogen isotopes in occluded air within ice cores (Methods; Figs S1 and S2)<sup>4</sup>. This method relies on temperature-dependent gas fractionation in the unconsolidated snow layer<sup>5</sup>. Temperature gradients between the top and bottom of the unconsolidated snow layer induce gas fractionation<sup>6</sup>. After which the fractionated gasses are trapped in ice at the bottom of the firn layer<sup>4</sup>. By measuring nitrogen and argon isotopes in ice cores, we can reconstruct past temperature gradients (Fig. S3)<sup>4</sup>, which combined with observed borehole temperature data and a firn densification/heat diffusion model, are used to reconstruct past surface temperature changes<sup>4,7,8</sup>. Reconstructed temperatures (Supplementary Dataset) are seasonally unbiased multidecadal average temperatures due to the processes of heat and gas diffusion in the firn layer<sup>4,5</sup>, and are constrained by borehole temperature profiles<sup>4</sup> (Method; Fig. S4). Sampling density is not constant through the Holocene such that uncertainty ranges of the reconstructed temperatures vary with time<sup>9</sup>.

<sup>1</sup>Climate and Environmental Physics, University of Bern, 3012, Bern, Switzerland. <sup>2</sup>Oeschger Centre for Climate Change Research, University of Bern, 3012, Bern, Switzerland. <sup>3</sup>Climate Change Research Centre and PANGAEA Research Centre, University of New South Wales, New South Wales, 2052, Australia. <sup>4</sup>ARC Centre of Excellence for Climate System Science, New South Wales, Sydney, Australia. <sup>5</sup>Centre for Ice and Climate, Niels Bohr Institute, University of Copenhagen, 2100, Copenhagen, Denmark. <sup>6</sup>Geological Survey of Greenland and Denmark, 1350, Copenhagen, Denmark. <sup>7</sup>Department of Geology, Quaternary Sciences, Lund University, 22362, Lund, Sweden. <sup>8</sup>Meteorological Research, Institute, Tsukuba, 305-0052, Ibaraki, Japan. <sup>9</sup>Institute for Atmospheric and Climate Science, Swiss Federal Institute of Technology ETH Zurich, 8092, Zurich, Switzerland. <sup>10</sup>Present address: Renewable Energy Institute, Minato-ku, 105-0003, Tokyo, Japan. Correspondence and requests for materials should be addressed to T.K. (email: [kobashi@climate.unibe.ch](mailto:kobashi@climate.unibe.ch))

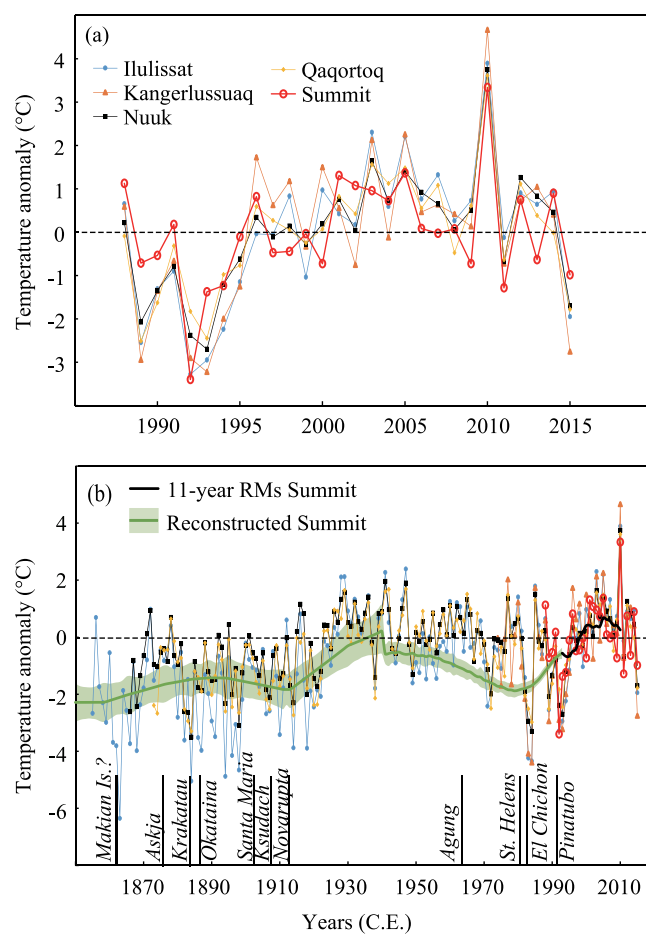


**Figure 1.** Greenland temperature anomalies relative to averages of 1988–2015 at the Summit and four coastal stations. **(a)** Temperature anomalies from 1988 to 2015. **(b)** Same as **(a)** but from 1850 to 2015. Green line with  $2\sigma$  error bands is the reconstructed temperature anomaly. The reconstructed temperature (snow temperature) was adjusted to have the same value in 1993 as an average of the observed Summit temperature (air temperature) for 1988–1998 by adding  $1.0^\circ\text{C}$ . The names and timings of large volcanic eruptions are according to Box *et al.*<sup>13</sup>. RMs represents running means.

Continuously observed instrumental Greenland Summit air temperature (GISP2) is now available for 28 years<sup>10</sup> (1988 to 2015; Fig. 1a), allowing us to place the current decadal average temperature into the long-term context of the Holocene. The record exhibits the characteristic temperature drop in 1992–1993 associated with cooling caused by the eruption of Mt. Pinatubo<sup>11</sup>, followed by an increase until 2005 (Fig. 1a). For the most recent 10 years (2005 to 2015), apart from the anomalously warm year of 2010, mean annual temperatures at the Summit exhibit a slightly decreasing trend in accordance with northern North Atlantic-wide cooling<sup>12</sup>. The Summit temperatures are well correlated ( $r \sim 0.7$ – $0.8$ ;  $p < 0.01$ ) with southwest coastal records (Ilulissat, Kangerlussuaq, Nuuk, and Qaqortoq; Fig. 1a). The high correlations between the Summit record and coastal temperatures allow us to use the longer coastal records to estimate Greenland Summit temperatures over the past 160 years (Fig. 1b). During this period, large volcanic eruptions caused 1 to 3 years cooling episodes in Greenland<sup>13</sup>. Importantly, the reconstructed nitrogen-argon-isotope-based temperatures (hereafter, reconstructed temperatures) agree well with the instrumental records on a multi-decadal scale (Fig. 1b).

The reconstructed temperatures exhibit a long-term trend similar to that of average  $\delta^{18}\text{O}_{\text{ice}}$  (GISP2<sup>14</sup>, GRIP and NGRIP; Fig. 2). However, the  $\delta^{18}\text{O}_{\text{ice}}$  records lack strong centennial to millennial-scale variability (e.g., the Medieval Climate Anomaly and Little Ice Age; Fig. 2). We find that 27% of the Holocene Greenland temperatures are higher than the present multi-decadal average (1988–2015, hereafter “the recent decades”; Figs 1 and 2a, Fig. S5). The reconstructed temperature reached the present level around 9,500 years B.P., which is earlier than that of the borehole based reconstruction (around 8,000 years B.P., Fig. 2). This is likely because borehole temperature reconstructions are unable to capture sharp transitions such as the one from the cold Younger Dryas to the warm Holocene due to the smoothing effect by diffusion of heat in the ice-sheet (Methods). Consistent with an earlier conclusion<sup>14,15</sup> from  $\delta^{18}\text{O}_{\text{ice}}$ , Greenland climate remained relatively stable and warm during the Holocene, compared to the highly variable and cold last glacial period (Fig. S6).

After an abrupt warming at the end of the Younger Dryas period, Greenland temperature gradually decreased toward the Holocene temperature minimum at  $11,271 \pm 30$  years B.P. ( $9.2 \pm 1.5^\circ\text{C}$  colder than the recent decades;

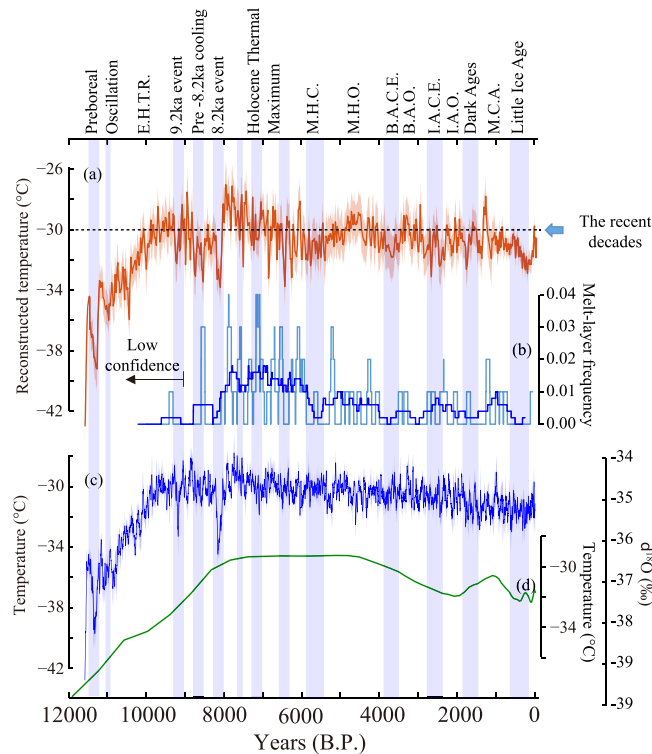


**Figure 2.** Greenland Summit temperature and its proxies over the Holocene. (a) Reconstructed temperature from argon and nitrogen isotopes with  $2\sigma$  error bands. (b) Melt-layer frequency (times per years) in 100 and 500-year RMs with light blue and blue lines, respectively. Note that the data before 9000 B.P. has low confidence<sup>20</sup>. (c)  $\delta^{18}\text{O}_{\text{ice}}$  and a calibrated temperature scale in 20-year RMs with  $2\sigma$  error bands from GISP2<sup>14</sup>, GRIP, and NGRIP<sup>15</sup> (Methods) (d) GRIP borehole temperature inversion<sup>12</sup>. Blue shades are Greenland cold episodes. E.H.T.R. = Early Holocene Temperature Rise, M.H.C. = Mid-Holocene Cooling, M.H.O. = Mid-Holocene Optimum, B.A.C.E. = Bronze Age Cold Epoch, B.A.O. = Bronze Age Optimum, I.A.C.E. = Iron Age Cold Epoch, I.A.O. = Iron Age Optimum, M.C.A. = Medieval Climate Anomaly. The names are given according to the Greenland temperature changes or common usages if available.

Preboreal Oscillation), which was followed by another abrupt warming (Figs 2 and 3)<sup>16</sup>. From 11,000 years B.P. to 9,500 years B.P., the temperature kept rising at a rate of  $3.7 \pm 0.1^\circ\text{C}$  per 1,000 years (Figs 2 and 3). At 9,200 years B.P., Greenland experienced a rapid cooling (9.2 ka event)<sup>17</sup>. Afterwards, the temperature gradually decreased with occasional large drops (Figs 2 and 3). Then, Greenland experienced the largest hemispheric-wide negative temperature excursion during the Holocene around 8,200 years B.P. (8.2 ka event)<sup>18,19</sup>.

After the 8.2 ka event, Greenland temperature reached the Holocene thermal maximum with the warmest decades occurring during the Holocene ( $2.9 \pm 1.4^\circ\text{C}$  warmer than the recent decades) at  $7960 \pm 30$  years B.P. Since then, the Summit temperature record exhibits a long-term cooling at a rate of  $0.19 \pm 0.01^\circ\text{C}$  per 1000 years towards the present ( $1.5 \pm 0.1^\circ\text{C}$  cooling in total), agreeing with other estimates from melt layer frequency ( $1.3^\circ\text{C}$ ) in GISP2 ice core<sup>20</sup> (Fig. 2b) and from the western Arctic ( $1.6 \pm 0.8^\circ\text{C}$ ; an average estimate of western Arctic cooling)<sup>21</sup>. Greenland experienced a temperature minimum around 5,500 years B.P. Afterwards, the temperature shows a slight increase for 1,500 years (Mid-Holocene Optimum), followed by a cooling into the Little Ice Age with occasional bumps (Fig. 2). From the coldest decades in the Little Ice Age (1740–1780 C.E.) to the recent decades, Greenland Summit temperature increased by  $2.9 \pm 0.9^\circ\text{C}$ .

The centennial to millennial-scale variability of the reconstructed Greenland temperature is significantly correlated with  $\text{Na}^+$  and  $\text{K}^+$  ion concentrations<sup>22,23</sup> from the GISP2 ice core, which are proxies for atmospheric circulation, as well as with the Oman and Dongge cave stalagmite  $\delta^{18}\text{O}$  records, proxies for monsoon activity, thus indicating that the reconstructed Greenland temperature variations contain hemispheric climate signals<sup>3,23</sup> (Methods; Fig. 4f–i). This is consistent with the observation that Greenland temperature generally followed proxy-based Northern Hemisphere (NH) average temperature changes over the past 2,000 years<sup>4</sup>.

To investigate possible causes of the temperature variability, we conducted a suite of climate model experiments with different sets of orbital, volcanic, solar, greenhouse gasses (GHG;  $\text{CO}_2$ ,  $\text{CH}_4$ , and  $\text{N}_2\text{O}$ ; Methods) forcings (Fig. 3e) as well as prescribed ice-sheet changes (i.e., ICE6G<sup>24</sup>; ice covered area, topography, and ice-sheet thickness) using the climate model of intermediate complexity, LOVECLIM<sup>25</sup> (Methods; Fig. 3). Volcanic forcing is reconstructed using the GISP2 sulfate record<sup>22</sup>, which agrees well with multi-core reconstructions<sup>26</sup> for centennial to millennial-scale variability during the overlapping period of the past 2,500 years (Methods; Fig. S7).

The experiments that include all forcings generally reproduce long-term Greenland temperature variations quite well with a cooling of  $0.17^\circ\text{C}/1000$  years since 7000 years B.P. (Fig. 3b). Five additional experiments were

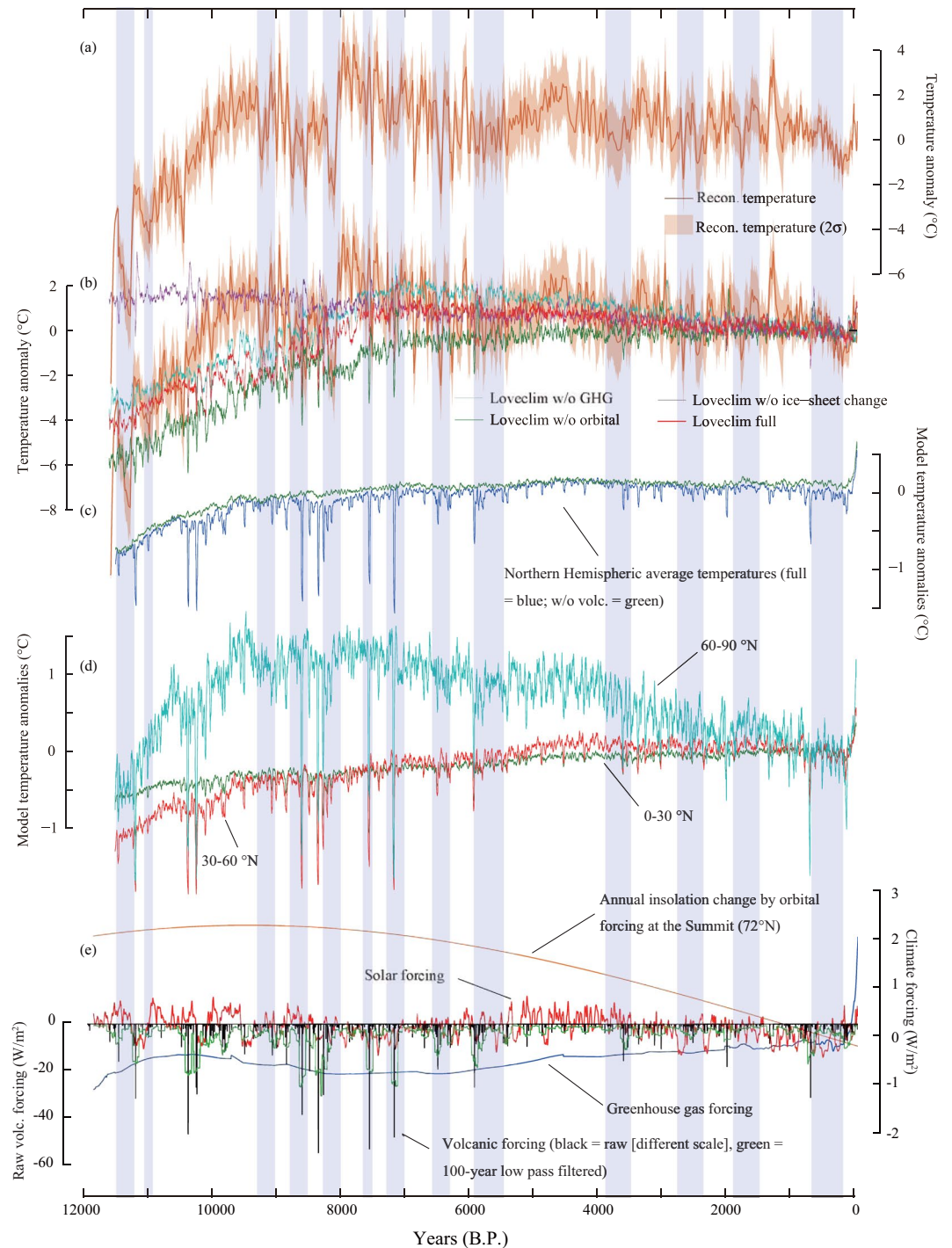


**Figure 3.** Holocene climate forcing. **(a)** Reconstructed Greenland temperature. **(b)** Reconstructed and modeled Greenland temperatures over the Holocene from various climate model experiments. Experiments without volcanic and solar forcing that exhibit long-term trends similar to that of full forcing are not shown for the sake of simplicity. **(c)** Modeled NH average temperatures with full forcing (blue) and without volcanic forcing (green) both relative to the average of the past 1000 years from the full forcing run. **(d)** Modeled high (60–90°N), middle (30–60°N), and low (0–30°N) latitude average temperatures. **(e)** Annual insolation at 72°N (orange)<sup>63</sup> and solar activity (red)<sup>31</sup>, GHG (blue; include CO<sub>2</sub>, CH<sub>4</sub>, and N<sub>2</sub>O, Methods) and volcanic forcing as raw (black) and 101-year RMs (green) (Methods). Note that the raw volcanic forcing has a different scale. Values are relative to averages of the past 1,000 years. Model outputs are from individual runs and smoothed by 21-year RMs. Blue shades are the Greenland cold episodes as in Fig. 2.

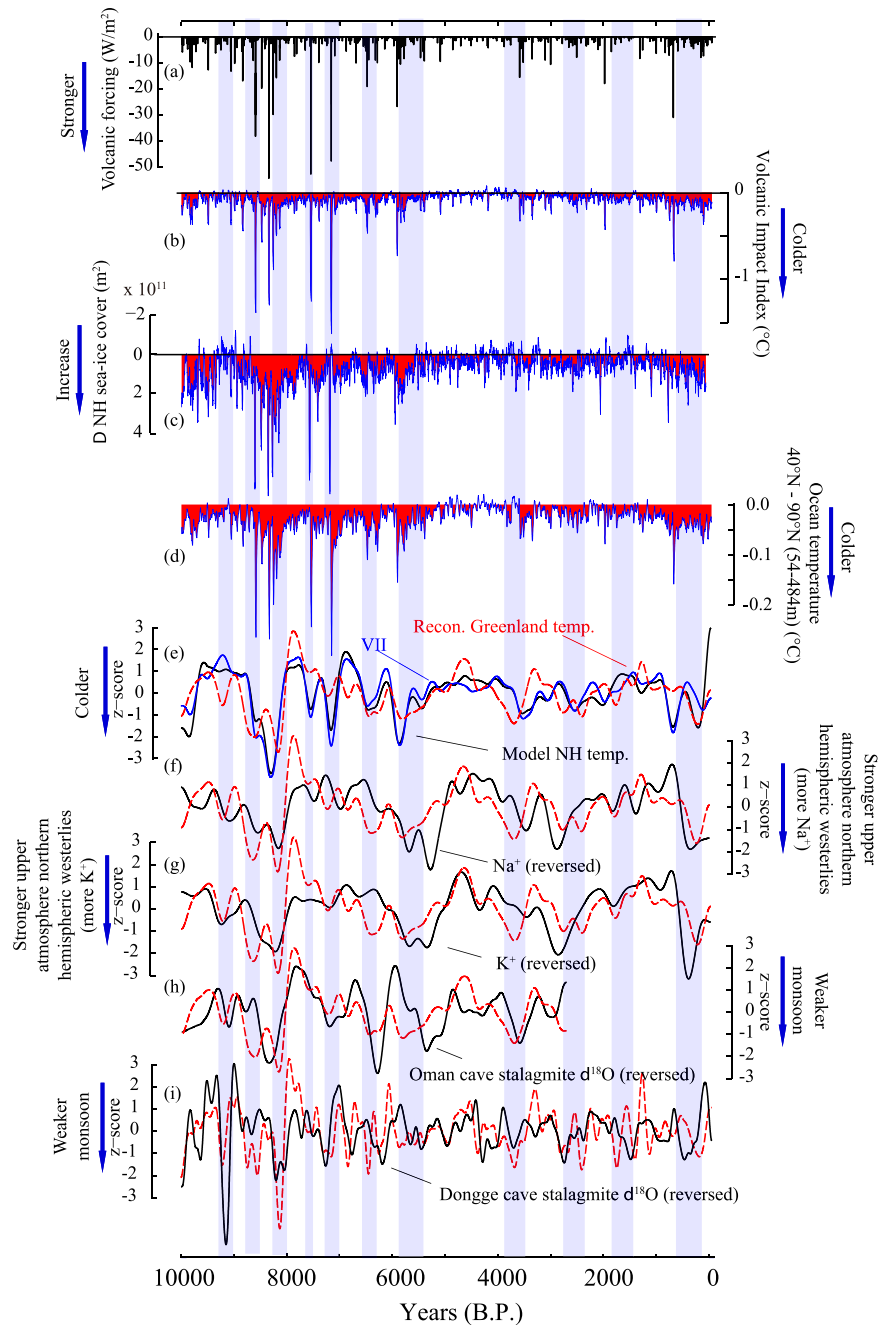


**Figure 4.** Centennial to millennial-scale volcanic impacts on climate over the past 10,000 years. (a) Raw volcanic forcing, (b) Volcanic Impact Index (VII), the difference between two curves in Fig. 3c. (c)  $\Delta$ NH sea-ice cover (y-axis is reversed) is calculated as differences between experiments with full forcing and without volcanic forcing (ensemble means) in 21-year RMs, (d) as in (c) but for ocean temperature (54–484 m) in 40°N–90°N. Red dotted lines in (e–i) show bandpass-filtered Greenland temperatures, which are compared to (e) modeled NH average temperatures (Methods), and VII, (f)  $\text{Na}^+$  ion in GISP2 (a proxy for atmospheric circulation)<sup>22</sup>, (g)  $\text{K}^+$  ion in GISP2 (proxy for atmospheric circulation)<sup>22</sup>, (h) Oman cave stalagmite  $\delta^{18}\text{O}$ <sup>1</sup>, (i) Dongge cave stalagmite  $\delta^{18}\text{O}$ <sup>64,65</sup>. Different bandpass filters were applied for (e,f,g,h) and (i) with 400–4000 year bands and 200–2000 year bands after linear detrending, respectively (Methods). Red areas in (b–d) indicate periods under relatively strong volcanic influence. Blue shades are the Greenland cold episodes as in Fig. 2.

conducted with sets of forcings that excluded one out of the GHG, orbital, volcanic, solar, and ice-sheet forcings at a time (Fig. 3b–d). An experiment with fixed present-day ice-sheet configuration indicates that the temperature rise from the beginning of the Holocene to 7,000 years B.P. was the result of the retreating Laurentide ice-sheet<sup>27</sup>, while the thinning of ice-sheet (~70 m)<sup>24</sup> played a minor role on the middle to late Holocene cooling (Fig. 3; Fig. S8).



In these simulations, meltwater inputs from retreating Northern Hemispheric ice-sheets were not taken into account. Particularly, through changes in ocean heat content, the Younger Dryas could have had an impact on temperature trends in the early Holocene (12,000–10,000 yrs B.P.). In addition, through weakening of the Atlantic Meridional Circulation and associated reduction in poleward oceanic heat transport, deglacial meltwater fluxes could have influenced the Northern hemispheric climate until 7,000 years B.P., and particularly during the 8.2 ka B.P. event<sup>28</sup>.

Two numerical experiments exhibit significantly different temperature trends from the middle Holocene to the present (Fig. 3b). From 7,000 years B.P. to the present, the experiment without orbital forcing displays a warming trend, whereas the simulation without GHG forcing overestimates the cooling trend. Therefore, the decreasing temperature trend from the middle to the late Holocene likely results from orbital forcing, but 43% of the orbitally induced cooling was compensated by the increasing GHG forcing (Fig. 3b). The reconstructed Greenland temperature and modeled NH average temperature are significantly correlated ( $r = 0.52$ ,  $p < 0.01$ ) on a centennial to millennial scale (400–4000 year band; Fig. 4e) over the past 10,000 years. The amplitude of temperature variability in simulated NH average temperature is small, but increases from low to high latitudes with amplified noises (Fig. 3d). Over 80% of the simulated hemispheric variability can be explained by volcanic forcing, as the millennial-scale variability (400–4000 year band) of NH temperature and volcanic impact index (VII = “NH average temperatures from full forcing experiments” minus “NH average temperature from no-volcanic forcing experiments” as in Figs 3c and 4b) are highly correlated ( $r = 0.90$ ,  $p < 0.001$ ) (Fig. 4e). Importantly, the VII has a significant correlation with the reconstructed Greenland temperature ( $r = 0.48$ ,  $p < 0.01$ ; Fig. 4e). As volcanic eruptions should not a-priori be related with changes in meltwater forcing, volcanic impacts on the variability of Greenland temperature do not exclude possible meltwater impacts (e.g., the 8.2 ka event<sup>28</sup>).

Recent studies indicate that large volcanic eruptions separated by several decades could induce decadal to centennial cooling in the northern hemisphere (e.g., Little Ice Age) by sea-ice/ocean feedbacks long after volcanic aerosols are removed from the atmosphere<sup>26,29</sup>. In our model experiments, volcanic impacts on climate show clear multi-decadal to millennial variabilities (Fig. 4), although the millennial signals are smaller than those found in the reconstructed temperatures (Fig. 3). The reduced magnitude of the millennial-scale signals in the model could partly be explained by the lack of a cryosphere component and thus potential positive feedbacks between the ice-sheet and ocean-atmosphere system.

In our simulations, a single large volcanic eruption induces rapid atmospheric and ocean surface cooling coupled with sea-ice expansion, which lasts about 16 years. However, slightly lower temperatures persist at high northern latitudes for a century or longer owing to decreased ocean temperatures, which affect ocean surface and sea-ice formation (Fig. 4a–d). Furthermore, a series of large volcanic eruptions (e.g., 9000–8000 years B.P. and the Little Ice Age) produces cold periods of centennial to millennial duration (Fig. 4a–d), which coincide with the reconstructed Greenland temperature decreases, stronger polar atmospheric circulation ( $[K^+]$  and  $[Na^+]$  in GISP2), and weaker Asian monsoon activity (Fig. 4e–i).

The period between 8,600 and 8,000 years B.P. featuring the most intense volcanic activity is also the one corresponding to strong meltwater outbreak from the Laurentide ice sheet<sup>28</sup> (Fig. 4). The beginning of the cooling started earlier than the rapid drop in  $\delta^{18}O_{ice}$  at 8,200 years B.P. (the 8.2 ka event; Figs 2 and 3). The pre-8.2 ka cooling has been found in many summer temperature proxies<sup>18</sup>, consistent with volcanically induced summer cooling. Therefore, the 8.2 ka cooling event<sup>18</sup> occurred during a longer-term cold period attributable to volcanic origin, which could have enhanced the sensitivity to meltwater outbreaks from the Laurentide ice sheet. We also note that the mid-Holocene Optimum (5,500–4,000 years B.P.) is characterized by a lack of large volcanic eruptions (Figs 3 and 4). After a period of intensive volcanism and associated cooling (6,000–5,800 years B.P.), a gradual return to a volcanically unperturbed state can be found in modeled 60–90°N average temperatures and in the reconstructed Greenland temperatures. Volcanic activity intensifies again towards the Little Ice Age. Only during the mid-Holocene Optimum were the ocean temperatures in the volcanically unperturbed state (Fig. 4), suggesting that the Holocene climate was mostly under the persistent influence of volcanic activity that is consistent with our earlier studies for the past 4000 years<sup>30</sup>.

Comparisons between the reconstructed Greenland temperatures, reconstructed solar irradiance (TSI)<sup>31</sup>, and model results indicate that solar variability did not play a persistent role in driving millennial-scale variability in Greenland. Nevertheless, solar variability had significant negative imprints on centennial temperature changes especially during the colder periods of the early and late Holocene (stronger solar activities induced colder temperatures in Greenland, or vice versa; Fig. S9) consistent with earlier studies<sup>4,32</sup>. Notably, periods of stronger solar activity in the early Holocene coincide with several rapid cooling periods (e.g., the Preboreal Oscillation and the 8.2 ka event; Fig. S9), indicating that abrupt climate change events during the Holocene may result from changes in several forcings (volcanic, solar, and meltwater inputs), with possible synergetic effects.

We reconstructed the seasonally unbiased and physically constrained Greenland temperature over the Holocene. In contrast to  $\delta^{18}O_{ice}$ , the reconstructed Greenland temperature exhibits clear centennial to millennial-scale variability, which is reproduced by climate model simulations including volcanic forcing. Large volcanic eruptions had sustained impacts on climate and people over the past 2,500 years<sup>26</sup>. Clearly, the volcanic impacts were not limited to the recent millennia, but persisted throughout the Holocene with possible important roles on human societal development.

## Methods

**Statistics.** To evaluate relationships of two time series, we applied the Pearson correlation coefficient. We consider autocorrelation of the time series to evaluate the significance of correlations by estimating the effective degree of freedom that depends on the effective decorrelation time<sup>33,34</sup>. Correlations or any statistics with >95% confidence levels are considered as significant. Reported uncertainty ranges are  $2\sigma$  standard deviation unless

otherwise stated. Z-score is a measure of a time series having mean zero and standard deviation of one. For filtering of the time series, we used a MATLAB function, “butter”.

**Chronology.** We used the Greenland ice core chronology (GICC05), which is based on annual layer counting from multiple cores, synchronized with common volcanic layers<sup>35,36</sup>. Recent studies indicated that GICC05 has slight offsets (up to 70 years<sup>37</sup> in the early Holocene) from true ages, or more precisely, from dendrochronologically-inferred calendar ages<sup>26,37,38</sup>. Therefore, we correct the offsets using the coefficients from Muscheler *et al.*<sup>37</sup>. The corrected chronology thus has a common time scale with <sup>14</sup>C-dated paleo records. For gas age calculations, we used a firn-densification and heat diffusion model<sup>39</sup> for the entire Holocene as an extension of the past 2,100 year calculation from our earlier study<sup>4</sup>. The agreement of timing of climate changes (e.g., the 8.2 ka event and Preboreal Oscillation) between  $\delta^{18}\text{O}_{\text{ice}}$  and the reconstructed temperature confirms the validity of the estimated gas ages.

**Temperature calculation.** Oxygen isotopes of ice ( $\delta^{18}\text{O}_{\text{ice}}$ ) have been widely used as a temperature proxy<sup>14,15</sup>, but  $\delta^{18}\text{O}_{\text{ice}}$  is influenced for example by seasonal changes of accumulation and water vapor source regions<sup>15,40,41</sup>. Borehole temperature reconstructions are a robust method to infer past temperatures, but their resolution decreases rapidly towards earlier ages<sup>42</sup>. Therefore, we have been developing a method to overcome drawbacks of existing temperature proxies using argon and nitrogen isotopes within occluded air in ice cores<sup>4,7–9,43</sup>.

The temperature calculation generally follows earlier studies for the past few millennia<sup>4,7</sup> with slight modifications for a longer period of the Holocene. We used argon and nitrogen isotope data over the Holocene from the GISP2 ice core<sup>9</sup>. Argon isotopes data requires a minor correction using  $\delta\text{Ar}/\text{N}_2$  data to compensate for possible fractionation during bubble close-off between open and closed pores<sup>7,8</sup>. However,  $\delta\text{Ar}/\text{N}_2$  data exhibit anomalous enrichments at brittle ice depths of a brittle zone (9,000–6000 years B.P.)<sup>9,43</sup>, which prohibited us from calculating the surface temperature through the Holocene until now. As we gained understanding of the  $\delta\text{Ar}/\text{N}_2$  fractionation in the firn layer<sup>43</sup>, it became possible to estimate pre-coring  $\delta\text{Ar}/\text{N}_2$  values<sup>43</sup> at the brittle zone by using accumulation rate<sup>44,45</sup> and  $\delta^{18}\text{O}_{\text{ice}}$ <sup>46</sup> data. For the argon isotope correction, we used  $\delta\text{Ar}/\text{N}_2$  data<sup>9</sup> for the past 6,000 years and the estimated  $\delta\text{Ar}/\text{N}_2$  for the earlier part of the Holocene. However, we found that the surface temperature reconstruction by correcting argon isotopes by a constant value (i.e., without  $\delta^{18}\text{O}_{\text{ice}}$  and accumulation rate) is essentially the same as the surface temperature reconstruction with argon isotopes corrected by the estimated  $\delta\text{Ar}/\text{N}_2$  using the  $\delta^{18}\text{O}_{\text{ice}}$  and accumulation rate. For the coefficient of argon isotope correction with  $\delta\text{Ar}/\text{N}_2$ , we applied the value (0.0073‰/‰) that was used for the temperature reconstruction over the past 4,000 years<sup>7</sup>.

Temperature gradients [ $\Delta T$  (°C) = ( $\delta^{15}\text{N} - \delta^{40}\text{Ar}/4$ )/ $k$ ] (Fig. S2) between the top and bottom of the firn layer<sup>6</sup> can be obtained from nitrogen and the corrected argon isotope data with the coefficient ( $k$ ) obtained from laboratory experiments<sup>47,48</sup>. The  $\Delta T$  data were splined<sup>49</sup> with a 51-year cutoff period (Fig. S3). Then, the data were again resampled for the sampling ages and used for the following calculations. Surface temperatures were calculated using a firn densification/heat diffusion model<sup>39</sup> by integrating the  $\Delta T$ s<sup>4,7,8</sup>. For a long integration of  $\Delta T$ , it is important to have precise  $\Delta T$  values as small errors could lead to drifts on the calculated surface temperatures during the integration. We circumvented the drifts by allowing slight constant shifts in  $\Delta T$  by minimizing the difference between the observed and modeled  $\delta^{15}\text{N}$ . The  $\Delta T$  integration was performed by dividing the Holocene into nine sections (about 1500-year intervals) including the sections of different measurement periods (e.g., different extraction setups<sup>9</sup>) to minimize the drift. We tested different sections and found little differences in the calculated surface temperatures. Observed and modelled  $\Delta T$ s agree within their uncertainties (Fig. S3).

The calculation started at 50,000 years B.P. to take a memory effect of temperature in the ice-sheet<sup>39</sup> into account. From 50,000 to 20,000 years B.P.,  $\delta^{18}\text{O}_{\text{ice}}$  was used as temperature after the calibration<sup>45,46</sup>. For the later period to the beginning of the Holocene (20,000 to 11,460 years B.P.), a temperature reconstruction from  $\delta^{15}\text{N}$  was used<sup>50</sup>. For both periods, slight constant shifts for prescribed temperatures were allowed to fit with borehole temperatures during the following minimization procedure. Surface temperature calculations are conducted automatically to minimize the differences between the modelled and observed  $\delta^{15}\text{N}$  and borehole temperature profiles with parameters (A, B) using a MATLAB function, “fminsearch” (Nelder-Mead simplex method)<sup>51</sup>. In total, 843 Greenland temperature time series were generated from different realizations of argon and nitrogen isotopic values produced within estimated errors<sup>4</sup>. For one realization, about 360 runs from 50,000 years B.P. to present were necessary with different values for each parameter. We further selected 646 realizations that have root mean square deviations of <0.0185‰ for the difference between the modeled and observed  $\delta^{15}\text{N}$  and <0.2 °C for the borehole temperature profiles. The 646 realizations were used to calculate mean and standard deviation of the reconstructed Greenland temperature. Comparisons between the calculated surface temperatures and raw  $\Delta T$  variations (calculated from  $\delta^{40}\text{Ar}$  not corrected for argon loss) indicate that most of the variability in the reconstructed temperature originates from the variability in raw  $\Delta T$  (Fig. S2). Argon corrections or surface temperature calculations only slightly influence the variability in the calculated surface temperature over the past 10,000 years (Fig. S2)<sup>4</sup>.

The temperature reconstruction from 1941 to 1993 C.E. was done using a borehole temperature inversion technique<sup>4</sup>, and a slight temperature shift at 1941 in Fig. 1 is due to the change in method. We also note that temperature calculations using only  $\delta^{15}\text{N}$ <sup>40,41</sup> produce somewhat different surface temperature histories. To capture small temperature changes such as those in the Holocene, high-precision nitrogen and argon data<sup>9</sup> and calculated temperature signals  $\Delta T$  are critical for the surface temperature calculation.

In Fig. 2, the reconstructed Greenland temperatures are compared with average  $\delta^{18}\text{O}_{\text{ice}}$  (GRIP, NGRIP, and GISP2). The average  $\delta^{18}\text{O}_{\text{ice}}$  has a temperature sensitivity of 0.36 permil/°C (geometric regression), and the correlation coefficient between the average  $\delta^{18}\text{O}_{\text{ice}}$  and temperature is  $r = 0.80$  ( $p = 0.01$ ). The reconstructed Greenland temperature vs  $\delta^{18}\text{O}_{\text{ice}}$  GRIP, NGRIP, and GISP2 has correlations of  $r = 0.76$  ( $p = 0.01$ ),  $0.76$  ( $p = 0.02$ ), and  $0.71$  ( $p = 0.01$ ), respectively. In Fig. 4, bandpass-filtered (400–4000 year bands) Greenland temperatures are compared

with modeled NH average temperatures ( $r = 0.52$ ,  $p < 0.01$ ), VII ( $r = 0.49$ ,  $p < 0.01$ ),  $\text{Na}^+$  ion in GISP2 ( $r = -0.49$ ,  $p = 0.01$ ),  $\text{K}^+$  ion in GISP2 ( $r = -0.51$ ,  $p < 0.01$ ), Oman cave stalagmite  $\delta^{18}\text{O}$  ( $r = -0.44$ ,  $p = 0.02$ ), Dongge cave stalagmite  $\delta^{18}\text{O}$  ( $r = -0.28$ ,  $p < 0.01$ ) that exhibits a significant correlation with the Greenland temperature in shorter periods (200–2000 year bands). The Dongge cave record has a less significant correlation ( $r = -0.23$ ,  $p = 0.12$ ) on 400–4000 year bands presumably because it is less influenced by North Atlantic climate. The bands were chosen to remove long term trends (e.g., orbital scale variation) and reduce noise.

**Climate model experiments.** We employed a three-dimensional Earth system model of intermediate complexity, LOVECLIM version 1.3<sup>25</sup>. The atmospheric component is ECbilt2, a T21, 3-level quasi-geostrophic model, fully coupled to the ocean general circulation model, CLIO3 (3° by 3° horizontal resolution, 20 vertical levels) and to the vegetation model, VECODE. To conduct transient experiments of the Holocene period, volcanic, solar, greenhouse gas and orbital<sup>52</sup> forcings were applied with variable ice-sheet configurations (ICE6G)<sup>24</sup>. For the solar forcing, we used a reconstruction of total solar irradiance (TSI) for the Holocene from tree-ring  $^{14}\text{C}$  data<sup>31</sup>. The greenhouse gas forcing includes  $\text{CO}_2$ <sup>53–55</sup>,  $\text{CH}_4$ <sup>56</sup>, and  $\text{N}_2\text{O}$ <sup>57</sup>, and concentration data are used as inputs in the model. The ice-sheet changes include extents, thickness (e.g., Greenland Ice-sheet), and ice covered area from the ICE 6 G database<sup>24</sup>. To precondition the ocean before the Holocene integration, an equilibrium simulation was conducted for 2,700 years with parameters for 20,000 years B.P., after which the model was transiently integrated towards the beginning of the Holocene with variable ice-sheets, greenhouse gas and orbital forcings (pre-Holocene run). A suite of Holocene experiments, initiated from 12,000 years B.P., were then performed with different sets of forcings. The initial conditions (a, b, c, and d) were derived from the end of the pre-Holocene run (12,000 years B.P.), and dates going back approximately 100 years apart from the end of the pre-Holocene run. We conducted four experiments with full forcings (initial conditions = a, b, c, and d), four experiments with full but without volcanic forcing (initial conditions = a, b, c, and d), and four experiments with full but without greenhouse gas, solar, orbital, or ice-sheet forcing.

**Volcanic forcing.** Volcanic forcing is generated from a sulfate concentration record of GISP2<sup>22</sup> and is an extension of the volcanic forcing generated for the study over the past 4,000 years<sup>30</sup>. The method<sup>30</sup> generally follows a study by Gao *et al.*<sup>58</sup>. The selected volcanic peaks are set to decay with an e-folding time of 1 year, approximating sulfate aerosol removal processes in the atmosphere<sup>30, 59</sup>. The GISP2 sulfate record has been used as a proxy for volcanic eruptions in numerous studies<sup>3, 60, 61</sup>. However, to our knowledge, this is the first study to use the record to produce volcanic forcing and run a climate model through the Holocene. The sulfate signals are linearly related to volcanic forcing. It has been indicated that sulfate loading in the atmosphere may become increasingly less effective to radiative forcing<sup>62</sup>. Therefore, linear relation may overestimate the size of the large eruptions.

We compared the volcanic forcing with more complete volcanic forcings from several studies using multi-ice cores<sup>26, 58</sup> (Fig. S7). For the past 1,500 years, the volcanic forcings from this study and Sigl *et al.*<sup>26</sup> (Fig. S7b,c) have a correlation of  $r = 0.78$ ,  $p = 0.0018$ , while this study vs. Gao *et al.*<sup>58</sup> has a correlation coefficient  $r = 0.86$ ,  $p = 0.0017$ , and Gao *et al.*<sup>58</sup> vs. Sigl *et al.*<sup>26</sup> have a correlation of  $r = 0.86$ ,  $p < 0.001$ . Therefore, over 70% of the total variance of volcanic forcing from multiple cores (Gao *et al.*) can be obtained by the single core (GISP2). For the past 2,500 years, this study and Sigl *et al.*<sup>26</sup> display a slightly lower correlation of  $r = 0.69$ ,  $p < 0.001$ , indicating that the reconstructed volcanic forcing obtained in this study well captures centennial to millennial trends of more complete volcanic forcings (Sigl *et al.*<sup>26</sup> and Gao *et al.*<sup>58</sup>). In addition, we note that during the periods of frequent large eruptions such as in the past 1,000 years, volcanic forcing reconstruction from a single core performs better than the periods of less frequent eruptions. The reconstructed volcanic forcing sometimes misses eruptions when compared with more complete reconstructions in raw data<sup>26</sup> (Fig. S7). Therefore our reconstruction is likely to be a lower-band estimate of true volcanic forcing. Also, we note that the strength of our volcanic forcing is located in the middle between Sigl *et al.*<sup>26</sup> and Gao *et al.*<sup>58</sup> reconstructions (Fig. S7), although the strength of true volcanic forcing is still under debate. In LOVECLIM, the volcanic forcing is implemented through anomalies in solar irradiance at the top of the atmosphere.

## References

- Fleitmann, D. *et al.* Holocene ITCZ and Indian monsoon dynamics recorded in stalagmites from Oman and Yemen (Socotra). *Quaternary Sci. Rev.* **26**, 170–188, doi:10.1016/j.quascirev.2006.04.012 (2007).
- Richerson, P. J. & Boyd, R. In *The Origin of Human Social Institutions, Proceedings-British Academy* Vol. 110 (ed. W. G. Runciman) 197–234 (Oxford University Press Inc., 2001).
- Mayewski, P. A. *et al.* Holocene climate variability. *Quaternary Res.* **62**, 243–255, doi:10.1016/j.yqres.2004.07.001 (2004).
- Kobashi, T. *et al.* Modern solar maximum forced late twentieth century Greenland cooling. *Geophys. Res. Lett.* **42**, 5992–5999, doi:10.1002/2015GL064764 (2015).
- Severinghaus, J. P., Grachev, A. & Battle, M. Thermal fractionation of air in polar firn by seasonal temperature gradients. *Geochim. Geophys. Res.* **2**, 1048–n/a, doi:10.1029/2000GC000146 (2001).
- Severinghaus, J. P., Sowers, T., Brook, E. J., Alley, R. B. & Bender, M. L. Timing of abrupt climate change at the end of the Younger Dryas interval from thermally fractionated gases in polar ice. *Nature* **391**, 141–146, doi:10.1038/34346 (1998).
- Kobashi, T. *et al.* High variability of Greenland surface temperature over the past 4000 years estimated from trapped air in an ice core. *Geophys. Res. Lett.* **38**, n/a–n/a, doi:10.1029/2011GL049444 (2011).
- Kobashi, T. *et al.* Persistent multi-decadal Greenland temperature fluctuation through the last millennium. *Climatic Change* **100**, 733–756, doi:10.1007/s10584-009-9689-9 (2010).
- Kobashi, T., Severinghaus, J. P. & Kawamura, K. Argon and nitrogen isotopes of trapped air in the GISP2 ice core during the Holocene epoch (0–11, 600 B.P.): Methodology and implications for gas loss processes. *Geochim. Cosmochim. Acta* **72**, 4675–4686, doi:10.1016/j.gca.2008.07.006 (2008).
- Cappelen, J. Greenland - DMI Historical Climate Data Collection 1784–2013, Denmark, The Faroe Islands and Greenland. 90 pp. (2014).
- Box, J. E. Survey of Greenland instrumental temperature records: 1873–2001. *Int. J. Climatol.* **22**, 1829–1847, doi:10.1002/(ISSN)1097-0088 (2002).



12. Robson, J., Ortega, P. & Sutton, R. A reversal of climatic trends in the North Atlantic since 2005. *Nature Geosc.* **9**, 513–517, doi:[10.1038/ngeo2727](https://doi.org/10.1038/ngeo2727) (2016).
13. Box, J. E., Yang, L., Bromwich, D. H. & Bai, L. S. Greenland Ice Sheet Surface Air Temperature Variability: 1840–2007. *J. Clim.* **22**, 4029–4049, doi:[10.1175/2009JCLI2816.1](https://doi.org/10.1175/2009JCLI2816.1) (2009).
14. Stuiver, M., Grootes, P. M. & Braziunas, T. F. The GISP2 delta O-18 climate record of the past 16,500 years and the role of the sun, ocean, and volcanoes. *Quaternary Res.* **44**, 341–354, doi:[10.1126/science.266.5192.1885](https://doi.org/10.1126/science.266.5192.1885) (1995).
15. Johnsen, S. J. *et al.* Oxygen isotope and palaeotemperature records from six Greenland ice core stations: Camp Century, Dye 3, GRIP, GISP2, Renland and NorthGRIP. *J. Quaternary Sci.* **16**, 299–307, doi:[10.1002/jqs.622](https://doi.org/10.1002/jqs.622) (2001).
16. Kobashi, T., Severinghaus, J. P. & Barnola, J. M.  $4 \pm 1.5^\circ\text{C}$  abrupt warming 11,270 years ago identified from trapped air in Greenland ice. *Earth Planet. Sc. Lett.* **268**, 397–407, doi:[10.1016/j.epsl.2008.01.032](https://doi.org/10.1016/j.epsl.2008.01.032) (2008).
17. Fleitmann, D. *et al.* Evidence for a widespread climatic anomaly at around 9.2 ka before present. *Paleoceanography* **23**, n/a–n/a, doi:[10.1029/2007PA001519](https://doi.org/10.1029/2007PA001519) (2008).
18. Rohling, E. J. & Pälike, H. Centennial-scale climate cooling with a sudden cold event around 8,200 years ago. *Nature* **434**, 975–979, doi:[10.1038/nature03421](https://doi.org/10.1038/nature03421) (2005).
19. Kobashi, T., Severinghaus, J., Brook, E. J., Barnola, J. M. & Grachev, A. Precise timing and characterization of abrupt climate change 8,200 years ago from air trapped in polar ice. *Quaternary Science Reviews*, doi:[10.1016/j.quascirev.2007.1001.1009](https://doi.org/10.1016/j.quascirev.2007.1001.1009) (2007).
20. Alley, R. B. & Anandakrishnan, S. Variations in melt-layer frequency in the GISP2 ice core: implications for Holocene summer temperatures in central Greenland. *Ann. Glaciol.* **21**, 64–70, doi:[10.1017/S0260305500015615](https://doi.org/10.1017/S0260305500015615) (1995).
21. Kaufman, D. *et al.* Holocene thermal maximum in the western Arctic (0–180 W). *Quaternary Sci. Rev.* **23**, 529–560, doi:[10.1016/j.quascirev.2003.09.007](https://doi.org/10.1016/j.quascirev.2003.09.007) (2004).
22. Mayewski, P. A. *et al.* Major features and forcing of high-latitude northern hemisphere atmospheric circulation using a 110,000-year-long glaciochemical series. *J. Geophys. Res.-Oceans* **102**, 26345–26366, doi:[10.1029/96JC03365](https://doi.org/10.1029/96JC03365) (1997).
23. O'Brien, S. R. *et al.* Complexity of Holocene Climate as Reconstructed from a Greenland Ice Core. *Science* **270**, 1962–1964, doi:[10.1126/science.270.5244.1962](https://doi.org/10.1126/science.270.5244.1962) (1995).
24. Peltier, W., Argus, D. & Drummond, R. Space geodesy constrains ice age terminal deglaciation: The global ICE-6G\_C (VM5a) model. *J. Geophys. Res.-Sol. Ea.* **120**, 450–487, doi:[10.1002/2014JB011176](https://doi.org/10.1002/2014JB011176) (2015).
25. Goosse, H. *et al.* Description of the Earth system model of intermediate complexity LOVECLIM version 1.2. *Geosci. model dev.* **3**, 603–633, doi:[10.5194/gmd-3-603-2010](https://doi.org/10.5194/gmd-3-603-2010) (2010).
26. Sigl, M. *et al.* Timing and climate forcing of volcanic eruptions for the past 2,500 years. *Nature* **523**, 543–549, doi:[10.1038/nature14565](https://doi.org/10.1038/nature14565) (2015).
27. Renssen, H., Seppä, H., Crosta, X., Goosse, H. & Roche, D. Global characterization of the Holocene thermal maximum. *Quaternary Sci. Rev.* **48**, 7–19, doi:[10.1016/j.quascirev.2012.05.022](https://doi.org/10.1016/j.quascirev.2012.05.022) (2012).
28. Kleiven, H. F. *et al.* Reduced North Atlantic Deep Water Coeval with the Glacial Lake Agassiz Freshwater Outburst. *Science* **319**, 60–64, doi:[10.1126/science.1148924](https://doi.org/10.1126/science.1148924) (2008).
29. Miller, G. H. *et al.* Abrupt onset of the Little Ice Age triggered by volcanism and sustained by sea-ice/ocean feedbacks. *Geophys. Res. Lett.* **39**, n/a–n/a, doi:[10.1029/2011GL050168](https://doi.org/10.1029/2011GL050168) (2012).
30. Kobashi, T., Goto-Azuma, K., Box, J. E., Gao, C.-C. & Nakaegawa, T. Causes of Greenland temperature variability over the past 4000 years: Implications for Northern Hemispheric temperature change. *Clim. Past* **9**, 2299–2317, doi:[10.5194/cp-9-2299-2013](https://doi.org/10.5194/cp-9-2299-2013) (2013).
31. Roth, R. & Joos, F. A reconstruction of radiocarbon production and total solar irradiance from the Holocene 14C and CO2 records: implications of data and model uncertainties. *Clim. Past* **9**, 1879–1909, doi:[10.5194/cp-9-1879-2013](https://doi.org/10.5194/cp-9-1879-2013) (2013).
32. Adolphi, F. *et al.* Persistent link between solar activity and Greenland climate during the Last Glacial Maximum. *Nature Geosc.* **7**, 662–666, doi:[10.1038/ngeo2225](https://doi.org/10.1038/ngeo2225) (2014).
33. Kobashi, T. *et al.* On the origin of Greenland temperature anomalies over the past 800 years. *Clim. Past* **9**, 583–596, doi:[10.5194/cp-9-583-2013](https://doi.org/10.5194/cp-9-583-2013) (2013).
34. Ito, H. & Minobe, S. *Data analysis for meteorology and physical oceanography*. (Meteorological Society of Japan, 2010).
35. Vinther, B. M. *et al.* A synchronized dating of three Greenland ice cores throughout the Holocene. *J. Geophys. Res.-Atmos.* **111**, doi:[10.1029/2005JD006921](https://doi.org/10.1029/2005JD006921) (2006).
36. Seierstad, I. K. *et al.* Consistently dated records from the Greenland GRIP, GISP2 and NGRIP ice cores for the past 104 ka reveal regional millennial-scale  $\delta^{18}\text{O}$  gradients with possible Heinrich event imprint. *Quaternary Sci. Rev.* **106**, 29–46, doi:[10.1016/j.quascirev.2014.10.032](https://doi.org/10.1016/j.quascirev.2014.10.032) (2014).
37. Muscheler, R., Adolphi, F. & Knudsen, M. F. Assessing the differences between the IntCal and Greenland ice-core time scales for the last 14,000 years via the common cosmogenic radionuclide variations. *Quaternary Sci. Rev.* **106**, 81–87, doi:[10.1038/ncomms9611](https://doi.org/10.1038/ncomms9611) (2014).
38. Adolphi, F. & Muscheler, R. Synchronizing the Greenland ice core and radiocarbon timescales over the Holocene – Bayesian wiggle-matching of cosmogenic radionuclide records. *Clim. Past* **12**, 15–30, doi:[10.5194/cp-12-15-2016](https://doi.org/10.5194/cp-12-15-2016) (2016).
39. Goujon, C., Barnola, J. M. & Ritz, C. Modeling the densification of polar firn including heat diffusion: Application to close-off characteristics and gas isotopic fractionation for Antarctica and Greenland sites. *J. Geophys. Res.-Atmos.* **108**, doi:[10.1029/2002JD003319](https://doi.org/10.1029/2002JD003319) (2003).
40. Kindler, P. *et al.* Temperature reconstruction from 10 to 120 kyr b2k from the NGRIP ice core. *Clim. Past* **10**, 887–902, doi:[10.5194/cp-10-887-2014](https://doi.org/10.5194/cp-10-887-2014) (2014).
41. Huber, C. *et al.* Isotope calibrated Greenland temperature record over Marine Isotope Stage 3 and its relation to CH<sub>4</sub>. *Earth Planet. Sc. Lett.* **243**, 504–519, doi:[10.1016/j.epsl.2006.01.002](https://doi.org/10.1016/j.epsl.2006.01.002) (2006).
42. Dahl-Jensen, D. *et al.* Past temperatures directly from the Greenland Ice Sheet. *Science* **282**, 268–271, doi:[10.1126/science.282.5387.268](https://doi.org/10.1126/science.282.5387.268) (1998).
43. Kobashi, T. *et al.* Post bubble-closeoff fractionation of gases in polar firn and ice cores: effects of accumulation rate on permeation through overloading pressure. *Atmos. Chem. Phys.* **15**, 1–20, doi:[10.5194/acp-15-13895-2015](https://doi.org/10.5194/acp-15-13895-2015) (2015).
44. Alley, R. B. *et al.* Visual-stratigraphic dating of the GISP2 ice core: Basis, reproducibility, and application. *J. Geophys. Res.-Oceans* **102**, 26367–26381, doi:[10.1029/96JC03837](https://doi.org/10.1029/96JC03837) (1997).
45. Cuffey, K. M. & Clow, G. D. Temperature, accumulation, and ice sheet elevation in central Greenland through the last deglacial transition. *J. Geophys. Res.-Oceans* **102**, 26383–26396, doi:[10.1029/96JC03981](https://doi.org/10.1029/96JC03981) (1997).
46. Stuiver, M. & Grootes, P. M. GISP2 oxygen isotope ratios. *Quaternary Res.* **53**, 277–284, doi:[10.1006/qres.2000.2127](https://doi.org/10.1006/qres.2000.2127) (2000).
47. Grachev, A. M. & Severinghaus, J. P. Determining the thermal diffusion factor for Ar-40/Ar-36 in air to aid paleoreconstruction of abrupt climate change. *J. Phys. Chem. A* **107**, 4636–4642, doi:[10.1021/jp027817u](https://doi.org/10.1021/jp027817u) (2003).
48. Grachev, A. M. & Severinghaus, J. P. Laboratory determination of thermal diffusion constants for N-29(2)/N-28(2) in air at temperatures from -60 to 0 degrees C for reconstruction of magnitudes of abrupt climate changes using the ice core fossil-air paleothermometer. *Geochim. Cosmochim. Ac.* **67**, 345–360, doi:[10.1016/S0016-7037\(02\)01115-8](https://doi.org/10.1016/S0016-7037(02)01115-8) (2003).
49. Enting, I. G. On the Use of Smoothing Splines to Filter CO<sub>2</sub> Data. *J. Geophys. Res.-Atmos.* **92**, 10977–10984, doi:[10.1029/JD092iD09p10977](https://doi.org/10.1029/JD092iD09p10977) (1987).
50. Buizert, C. *et al.* Greenland temperature response to climate forcing during the last deglaciation. *Science* **345**, 1177–1180, doi:[10.1126/science.1254961](https://doi.org/10.1126/science.1254961) (2014).

51. Lagarias, J. C., Reeds, J. A., Wright, M. H. & Wright, P. E. Convergence properties of the Nelder–Mead simplex method in low dimensions. *SIAM J. Optimiz.* **9**, 112–147, doi:[10.1137/S1052623496303470](https://doi.org/10.1137/S1052623496303470) (1998).
52. Berger, A. L. Long-term variations of daily insolation and Quaternary climatic changes. *J. Atmos. Sci.* **35**, 2362–2367 (1978).
53. Monnin, E. *et al.* Evidence for substantial accumulation rate variability in Antarctica during the Holocene, through synchronization of CO<sub>2</sub> in the Taylor Dome, Dome C and DML ice cores. *Earth Planet. Sc. Lett.* **224**, 45–54, doi:[10.1016/j.epsl.2004.05.007](https://doi.org/10.1016/j.epsl.2004.05.007) (2004).
54. Monnin, E. *et al.* Atmospheric CO<sub>2</sub> concentrations over the last glacial termination. *Science* **291**, 112–114, doi:[10.1126/science.291.5501.112](https://doi.org/10.1126/science.291.5501.112) (2001).
55. Siegenthaler, U. *et al.* Supporting evidence from the EPICA Dronning Maud Land ice core for atmospheric CO<sub>2</sub> changes during the past millennium. *Tellus B* **57**, 51–57, doi:[10.3402/tellusb.v57i1.16774](https://doi.org/10.3402/tellusb.v57i1.16774) (2005).
56. Brook, E. J., Sowers, T. & Orchard, J. Rapid variations in atmospheric methane concentration during the past 110,000 years. *Science* **273**, 1087–91, doi:[10.1126/science.273.5278.1087](https://doi.org/10.1126/science.273.5278.1087) (1996).
57. Sowers, T., Alley, R. B. & Jubenville, J. Ice core records of atmospheric N<sub>2</sub>O covering the last 106,000 years. *Science* **301**, 945–948, doi:[10.1126/science.1085293](https://doi.org/10.1126/science.1085293) (2003).
58. Gao, C., Robock, A. & Ammann, C. Volcanic forcing of climate over the past 1500 years: An improved ice core-based index for climate models. *J. Geophys. Res.-Atmos.* **113**, D23111, doi:[10.1029/2008JD010239](https://doi.org/10.1029/2008JD010239) (2008).
59. Robock, A. Volcanic eruptions and climate. *Rev. Geophys.* **38**, 191–219, doi:[10.1029/1998RG000054](https://doi.org/10.1029/1998RG000054) (2000).
60. Wanner, H. *et al.* Mid- to late Holocene climate change: an overview. *Quaternary Sci. Rev.* **27**, 1791–1828, doi:[10.1016/j.quascirev.2008.06.013](https://doi.org/10.1016/j.quascirev.2008.06.013) (2008).
61. Zielinski, G. A. *et al.* Record of volcanism since 7000 BC from the GISP2 Greenland ice core and implications for the volcano-climate system. *Science* **264**, 948–952, doi:[10.1126/science.264.5161.948](https://doi.org/10.1126/science.264.5161.948) (1994).
62. Crowley, T. J. & Unterman, M. B. Technical details concerning development of a 1200 yr proxy index for global volcanism. *Earth Syst. Sci. Data* **5**, 187–197, doi:[10.5194/essd-5-187-2013](https://doi.org/10.5194/essd-5-187-2013) (2013).
63. Laskar, J. *et al.* A long-term numerical solution for the insolation quantities of the Earth. *Astron. Astrophys.* **428**, 261–285, doi:[10.1051/0004-6361:20041335](https://doi.org/10.1051/0004-6361:20041335) (2004).
64. Dykoski, C. A. *et al.* A high-resolution, absolute-dated Holocene and deglacial Asian monsoon record from Dongge Cave, China. *Earth Planet. Sc. Lett.* **233**, 71–86, doi:[10.1016/j.epsl.2005.01.036](https://doi.org/10.1016/j.epsl.2005.01.036) (2005).
65. Wang, Y. J. *et al.* The Holocene Asian monsoon: Links to solar changes and North Atlantic climate. *Science* **308**, 854–857, doi:[10.1126/science.1106296](https://doi.org/10.1126/science.1106296) (2005).

## Acknowledgements

We thank H. Goosse for advice on LOVECLIM experiments. The project is supported by the E.U. Marie Curie Fellowship (624183; Greentemp) to T.K.L. Meniel acknowledges funding from the Australian Research Council grant DE150100107. J.E.B. was supported by Geocenter Denmark.

## Author Contributions

T.K. conceived the project, and wrote the paper. T.K. conducted Greenland temperature reconstruction with M.D., M.L., and the data analyses with A.J.-T., T.K. performed climate model simulations with P.L.P., L.M., and T.N., and analyzed the data with L.M., J.E.B. provided instrumental air temperature records. B.M.V. prepared  $\delta^{18}\text{O}_{\text{ice}}$ . R.M., H.W. and A.O. supported climate interpretation. All authors contributed on interpreting climate data, and improving the final manuscript.

## Additional Information

**Supplementary information** accompanies this paper at doi:[10.1038/s41598-017-01451-7](https://doi.org/10.1038/s41598-017-01451-7)

**Competing Interests:** The authors declare that they have no competing interests.

**Publisher's note:** Springer Nature remains neutral with regard to jurisdictional claims in published maps and institutional affiliations.



**Open Access** This article is licensed under a Creative Commons Attribution 4.0 International License, which permits use, sharing, adaptation, distribution and reproduction in any medium or format, as long as you give appropriate credit to the original author(s) and the source, provide a link to the Creative Commons license, and indicate if changes were made. The images or other third party material in this article are included in the article's Creative Commons license, unless indicated otherwise in a credit line to the material. If material is not included in the article's Creative Commons license and your intended use is not permitted by statutory regulation or exceeds the permitted use, you will need to obtain permission directly from the copyright holder. To view a copy of this license, visit <http://creativecommons.org/licenses/by/4.0/>.

© The Author(s) 2017